Nuclear Instruments and Methods in Physics Research A 1069 (2024) 169946

Contents lists available at ScienceDirect

Nuclear Inst. and Methods in Physics Research, A

journal homepage: www.elsevier.com/locate/nima

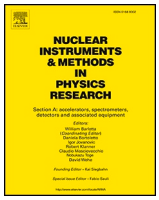

Design and application of a shipborne underwater radiation detector array for the monitoring of seawater radioactivity

Yihang Shou [a], Pin Gong [a,b,*], Jinzhao Zhang [c], Zeyu Wang [a], Dajian Liang [a], Cheng Zhou [d], Xiaobin Tang [a,b,**]

[a] Department of Nuclear Science and Technology, Nanjing University of Aeronautics and Astronautics, Nanjing, 210016, China
[b] Key Laboratory of Nuclear Technology Application and Radiation Protection in Aerospace, Ministry of Industry and Information Technology, Nanjing University of Aeronautics and Astronautics, Nanjing, 210016, China
[c] Third Institute Oceanography Ministry of Natural Resources, Xiamen, 361005, China
[d] Jiangsu Nuclear and Radiation Safety Supervision and Management Center, Nanjing, 210019, China

ARTICLE INFO

Keywords:
Shipborne marine radioactivity measurement
γ-ray spectrometry
Monte Carlo simulation
NaI(Tl) detector array

ABSTRACT

A navigable online monitoring system for marine radioactivity was developed to cope with possible large-scale marine nuclear pollution incidents. This system used a NaI(Tl) detector array mounted on a ship to collect radioactive data across wide marine areas rapidly. High volume-efficiency aids the system in rapidly identifying radionuclides exceeding standard levels. This feature enables the system to monitor the seawater in a wide area within a shorter time and promptly detect marine nuclear pollution incidents. Monte Carlo simulations were used to optimize the number of NaI(Tl) crystals and the detector spacing for enhancing the volume-efficiency of the system. Three Φ3" × 6″ NaI(Tl) detectors and the mounting bracket with a fixed detector spacing of 30 cm were fabricated based on the simulation outcomes. The volume-efficiency for ^{137}Cs of the system was around six times higher than that for the buoy-based monitoring system with a 3-inch NaI(Tl) detector. The theoretical volume-efficiency curve, which was calculated through Monte Carlo simulation, was verified in a standard liquid source. The minimum detectable activity concentration (MDC) for radioisotopes of the system under various radioactive measurement durations was discussed, such as the MDC for ^{137}Cs for 5 min measurement was 0.152 Bq/L. Marine radioactivity measurement experiments were conducted in the sea near the Tianwan nuclear power plant in Lianyungang, China. The test results showed that the activity concentration of ^{40}K was 11.4 Bq/L. The results of navigation monitoring were consistent with those of sampling and laboratory measurement, which verified the stability and accuracy of the system.

1. Introduction

Accidents in coastal nuclear power plants and maritime nuclear submarines can result in widespread radioactive pollution of seawater [1–3]. For example, Japan discharged nuclear wastewater from the Fukushima nuclear power plant into the ocean on August 24, 2023, which raised concerns regarding potential impacts on marine ecosystems [4]. The need for marine radiation monitoring has become increasingly apparent. Currently, the commonly used methods for monitoring marine radioactive pollution are manual sampling monitoring and buoy-based in situ monitoring. Manual sampling requires monitoring personnel to collect seawater samples at designated locations and then transport them back to the laboratory for analysis. Although this method is highly sensitive, it is limited by the lack of real-time capability [5–8]. Buoy-based in situ monitoring commonly involves the deployment of 3-inch NaI(Tl) detectors on buoys for real-time monitoring of seawater at specific points. However, the application of these methods to wide-area monitoring requires many buoys, which is challenged by high construction costs and maintenance [9–13].

A navigable online monitoring system was developed in this study for real-time monitoring of large-scale seawater radioactivity. As shown in Fig. 1, the system was equipped with an underwater radiation detector array composed of multiple large-volume NaI(Tl) detectors

* Corresponding author.
** Corresponding author. Department of Nuclear Science and Technology, Nanjing University of Aeronautics and Astronautics, Nanjing, 210016, China.
E-mail addresses: gongpin@nuaa.edu.cn (P. Gong), tangxiaobin@nuaa.edu.cn (X. Tang).

https://doi.org/10.1016/j.nima.2024.169946
Received 5 August 2024; Received in revised form 20 September 2024; Accepted 29 September 2024
Available online 30 September 2024
0168-9002/

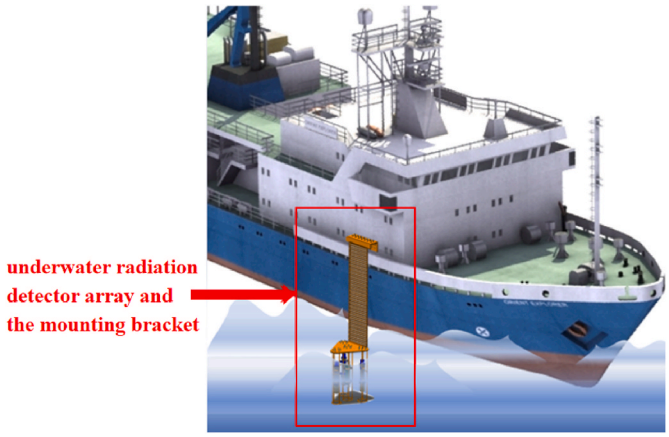

Fig. 1. Installation method of the detector array. The detector array is submerged in seawater during navigation.

mounted on a ship to collect seawater radioactivity data during navigation. The seawater radioactivity measurement is a type of volume source detection. The detection efficiency is related to the volume of seawater. To distinguish it from traditional detection efficiency, this paper refers to it as volume efficiency. When the volume-efficiency of the system is higher, the time required to respond to radionuclides exceeding standard levels increases. This condition helps the system monitor seawater in a wide area rapidly and discover nuclear accidents in a timely manner. Therefore, the design of the underwater radiation detector array needs to be optimized to improve the volume-efficiency of the system. This study describes the design of the detector array and the measurement results from the field experiments in the sea near the Tianwan nuclear power plant.

2. Design of underwater radiation detector array

2.1. MCNP model of the underwater radiation detector array

The technology based on NaI(Tl) scintillation crystals is currently the primary method employed in marine radioactivity monitoring [14,15]. The crystals with larger volumes are characterized by higher volume-efficiency, which aids in the early identification of nuclear accidents. Therefore, the NaI(Tl) detector array with a total crystal volume of 127.2 cubic inches, which is equivalent to the sum of six Φ3" × 3″ crystals, was utilized in this work. The MCNP code was adopted to further improve the volume-efficiency of the system. The code was utilized to simulate the effects of the number of NaI(Tl) crystals and detector spacing on volume-efficiency under the condition of constant total crystal volume. The goal was to optimize the design of the NaI(Tl) detector array.

The structure of the detector is shown in Fig. 2. The NaI(Tl) crystal and the outer casing were cylindrical. Above the crystal was an air layer

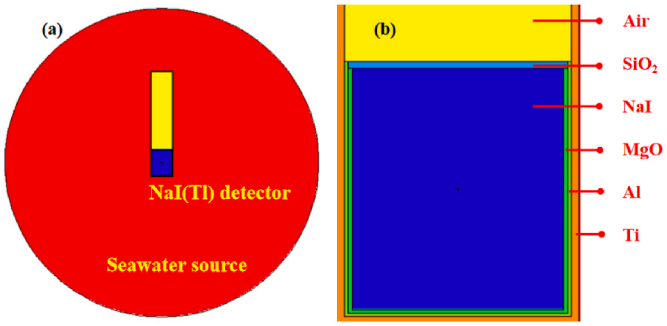

Fig. 2. MCNP model of the NaI(Tl) detector.

with a height of 50.21 cm. Below the air layer, a 0.5 cm thick SiO_2 layer was present, followed by a 0.25 cm thick MgO layer and a 0.2 cm thick Al layer. The outer shell was made of Ti alloy with a thickness of 0.5 cm.

In this study, the NaI(Tl) crystal with a constant total volume was divided into n quantities, where n ranged from 1 to 6 (Table 1). While the dimensions of the crystals in the detectors were changed, the thickness of other materials, such as MgO, Al, SiO_2, and Ti, and the height of the air layer were kept constant.

The source model was configured as spherical. Radioactive nuclides were assumed to have a uniform distribution in seawater. The detector was at the center of spherical seawater. Under these geometric conditions, the volume-efficiency ε_V was calculated using Formula (1):

$$\varepsilon_V = V \times \varepsilon \tag{1}$$

where V is the simulated seawater volume in L, and full energy peak ε is simulated using the pulse height tally 'F8:P′ with the default physics option in the MCNP code. The unit of the volume-efficiency ε_V is cps/(Bq/L).

This study determined the size of the seawater volume source based on detection distance to simulate the large seawater radiative environment; this distance was defined as the farthest distance at which the detector could detect gamma rays [16]. The Monte Carlo model, as shown in Fig. 2(a), positioned a single detector within a spherical seawater source. In the model, the center of the sphere coincided with the NaI(Tl) crystal center. A total of 12 values collected at intervals of 10 cm from 10 cm to 120 cm were used as the radius of the sphere. The curves in Figs. 3 and 4 show the volume-efficiencies of NaI(Tl) detectors of different specifications for the 0.662 MeV gamma rays from ^{137}Cs and the 2.62 MeV gamma rays from ^{208}Tl. The efficiencies vary with the radius of spherical seawater sources.

The results indicated that, with the increase in sphere radius, the volume-efficiency initially rose first and then stabilized. The smallest source radius at which the volume-efficiency reaches its maximum was considered the effective detection distance. When the volume of a single NaI(Tl) crystal increased or the energy of the radiation rose, the effective detection distance amplified. For a NaI(Tl) detector with dimensions of Φ5" × 6.5″ inches, the maximum detection distance for 2.62 MeV gamma rays was 100 cm. The distance from the boundary of the seawater sphere source to the center of the NaI(Tl) crystal should be at least 100 cm in this study.

2.2. Effect of detector spacing on volume-efficiency

In the detector array, the detector spacing, which was defined as the minimum distance between the surfaces of the housings of two adjacent detectors, may affect the volume-efficiency. Therefore, the detector spacing needs to be optimized to improve volume-efficiency. The MCNP model is shown in Fig. 5, where the centers of the NaI(Tl) crystals were situated on the same plane to ensure that the detectors were at the same height, and their geometric centers were aligned with the center of the sphere. The detector array was arranged in a symmetric polygonal pattern to ensure structural stability during navigation. A total of 7 spacing values collected at intervals of 10 cm from 0 cm to 60 cm were used as the detector spacing, and the radius of the seawater source was set to 200 cm.

Table 1
Dimensions of NaI(Tl) crystals.

Number of NaI(Tl) crystals	Dimensions of crystals
1	Φ5" × 6.5″
2	Φ4" × 5.1″
3	Φ3" × 6″
4	Φ3" × 4.5″
5	Φ3" × 3.6″
6	Φ3" × 3″

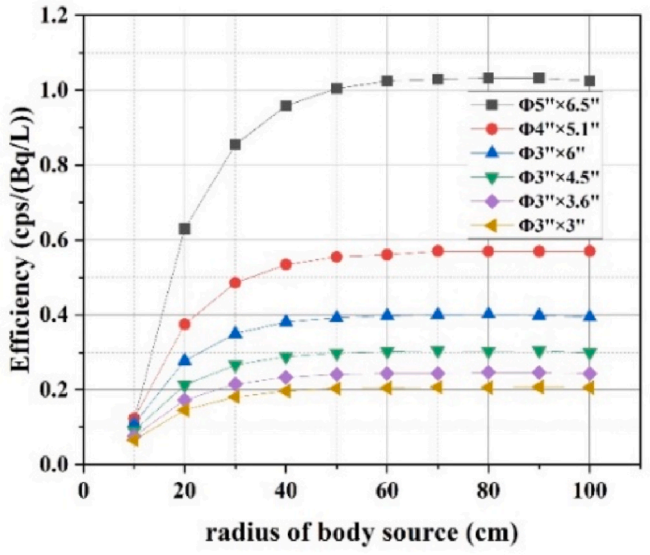

Fig. 3. Volume-efficiency for 0.662 MeV γ rays as a function of source radius.

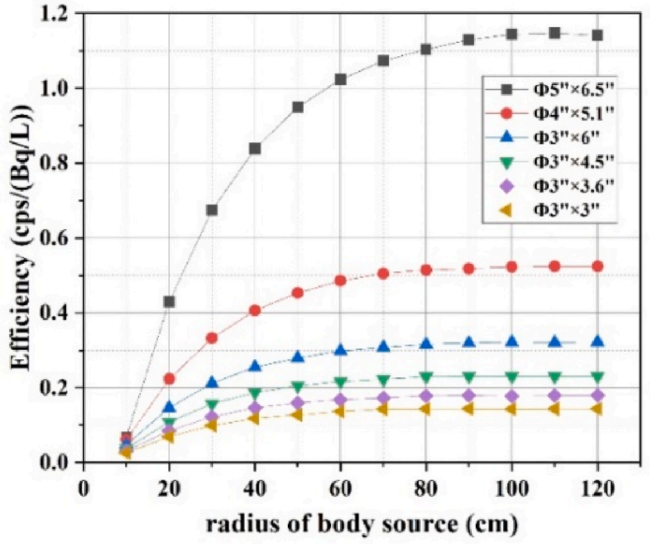

Fig. 4. Volume-efficiency for 2.62 MeV γ rays as a function of source radius.

The curves in Figs. 6 and 7 illustrate the volume-efficiency of different combinations of detector arrays for 0.662 and 2.62 MeV gamma rays as a function of detector spacing. The curves exhibited similar trends, with volume-efficiency initially increased as spacing rose. When the spacing exceeded 30 cm, the volume-efficiency reached a maximum and tended to stabilize. Given that the detectors in the detector array will obstruct gamma rays from each other, a shielding effect will be generated, which reduces the volume-efficiency. Once the spacing reaches 30 cm, the shielding effect between them nearly disappears. Therefore, the detector spacing in the array should be greater than or equal to 30 cm for the monitoring of seawater radioactivity.

2.3. *Effect of the number of NaI(Tl) crystals on volume-efficiency*

This section simulated volume-efficiency curves for different combinations of detector arrays. The aim was to determine the optimal number of NaI(Tl) crystals based on the total volume-efficiency within the energy range of 0.05–3 MeV and the sum of the volume-efficiency for major artificial radionuclides discharged into the ocean from nuclear power plants.

The model for optimizing the number of NaI(Tl) crystals, similar to Fig. 5(b), used a fixed detector spacing of 30 cm and a seawater sphere source radius of 200 cm. The source energy ranged from 0.05 MeV to 3 MeV, with intervals of 0.1 MeV. As a result, 31 energy values were

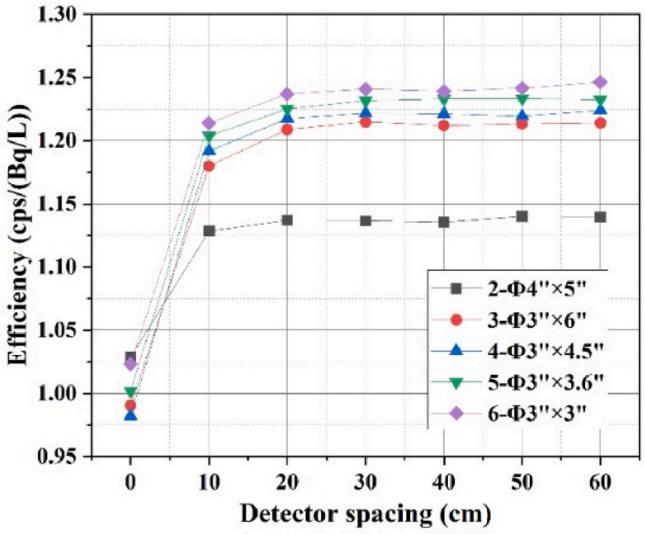

Fig. 6. Relationship between detector spacing and volume-efficiency for 0.662 MeV gamma rays.

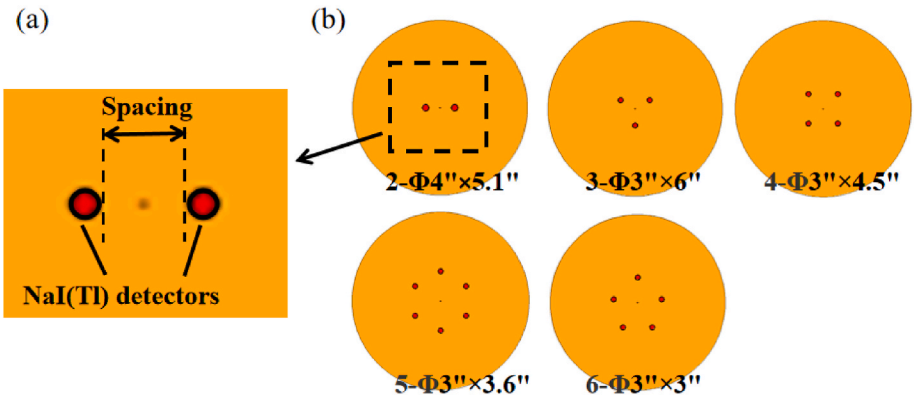

Fig. 5. (a) Detector spacing (b) Top-down MCNP view of various combinations of detector arrays. The yellow section represents the seawater, and the red depicts NaI (Tl) detectors.

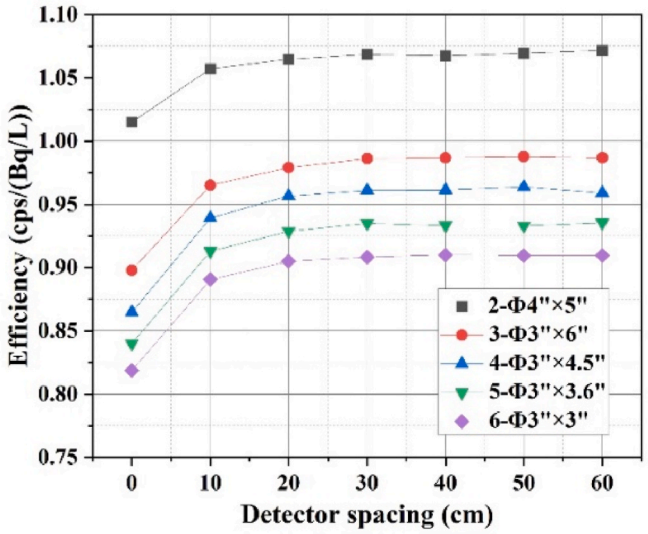

Fig. 7. Relationship between detector spacing and volume-efficiency for 2.62 MeV gamma rays.

generated. The volume-efficiency curve was fitted using Formula (2).

$$\ln \varepsilon_V = \sum_i P_i (\ln E)^i \tag{2}$$

where E represents the particle energy, ε_V denotes the volume-efficiency, i ranges from 0 to 6, and P_i represents the parameters to be calculated. The volume-efficiency curves for different combinations of detector arrays are shown in Fig. 8.

In Fig. 8, the volume-efficiency curves initially rose and then declined with the increase in energy. With the increase in gamma-ray energy, the effective detection distance, which was defined as the farthest distance at which the detector can detect gamma rays, rose. This improvement led to a higher number of particles detected by the detector, which boosted the volume-efficiency. However, as the gamma-ray energy increased, the probability of complete energy deposition within the crystal decreased, which resulted in the decline in volume-efficiency for full-energy peaks. At higher energies, the dominant effect was the decrease in energy deposition probability, which led to a reduction in volume-efficiency. Conversely, at lower energies, the increase in counting rate dominated, which improved the volume-efficiency.

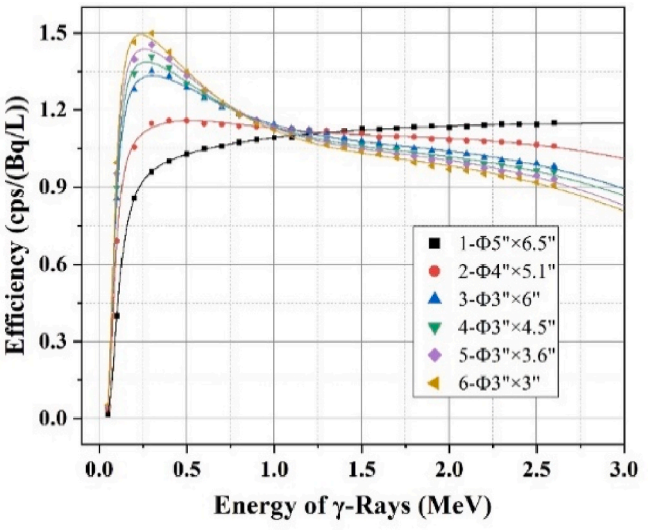

Fig. 8. Volume-efficiency curves for different combinations of detector arrays.

Fig. 8 also shows that the volume-efficiency curves intersected pairwise. Before these intersections, the detector array with more NaI (Tl) crystals had higher volume-efficiency, while the opposite was true after the intersections. Given the consistency in the total volume of crystals, the volume-efficiency curves for different combinations of detector arrays will exhibit a point of intersection. At this intersection, the decrease in volume-efficiency due to the reduction in the volume of each crystal is balanced by the increase in volume-efficiency resulting from more crystals. In the high-energy region after the intersection point, the decrease in volume-efficiency due to reducing the volume of individual crystals has a greater impact on detecting high-energy particles than the effects of increasing the number of crystals. Therefore, the detector array with fewer NaI(Tl) crystals but larger individual crystal volumes had higher volume-efficiency. Conversely, in the low-energy region, increasing the number of NaI(Tl) crystals has a larger impact on enhancing the volume-efficiency of low-energy photons. Therefore, the detector array with more NaI(Tl) crystals achieved higher volume-efficiency in the low-energy region.

The total volume-efficiency in the energy range of 0.05–3 MeV and the sum of volume-efficiencies for the major artificial nuclides emitted from nuclear power plants are shown in Table 2. The results indicated that detector arrays with 2, 3, and 4 NaI(Tl) crystals exhibited higher overall volume-efficiency in the range of 0.5–3 MeV. The sum of volume-efficiency for major nuclides in detector arrays with 3, 4, 5, and 6 NaI (Tl) crystals was higher. Comparing the two parameters showed that, for NaI(Tl) crystals with a total volume of 127.2 cubic inches, dividing them into 3 or 4 equal-volume crystals and arranging them in a detector array with a detector spacing of 30 cm or more was optimal for the monitoring of seawater radioactivity. The volume-efficiency for ^{137}Cs of the detector array composed of three Φ3" × 6″ NaI(Tl) detectors reached 1.22 cps/(Bq/L) and was about six times higher than the 0.21 cps/(Bq/L) from a buoy-based gamma-ray measurement system with a Φ3" × 3″ NaI(Tl) detector as this study [13]. The results also showed that the optimized design of the large volume NaI(Tl) detector array could improve the volume-efficiency of the system, which resulted in quicker responses of the system to nuclear accidents.

3. Deployment tests of the underwater radiation detector array in marine environment

3.1. Online monitoring system for navigable marine radioactivity

Based on the simulation results from Chapter 2, three Φ3" × 6″ NaI (Tl) detectors were fabricated and assembled into an underwater radiation detector array. The mounting bracket with a fixed detector spacing of 30 cm was designed, as shown in Fig. 9. The length of the bracket could be adjusted to position the centers of the crystals below the sea surface by 100 cm.

The hydrostatic pressure test of the NaI (Tl) detectors was carried out at the National Ocean Technology Center, China. The NaI(Tl) detectors

Table 2
Parameters for comparing volume-efficiency.

Different combinations of detector arrays	Sum of volume-efficiencies at 0.05–3 MeV cps/(Bq/L)	Sum of volume-efficiencies for major artificial nuclides emitted from nuclear power plants[a] cps/(Bq/L)
1-Φ5" × 6.5″	3.17E+04	14.99
2-Φ4" × 5.1″	3.19E+04	15.86
3-Φ3" × 6″	3.20E+04	16.57
4-Φ3" × 4.5″	3.18E+04	16.58
5-Φ3" × 3.6″	3.17E+04	16.69
6-Φ3" × 3″	3.15E+04	16.67

[a] Major artificial nuclides emitted from nuclear power plants [17]: ^{51}Cr, ^{54}Mn, ^{59}Fe, ^{58}Co, ^{60}Co, ^{134}Cs, ^{137}Cs, ^{131}I, ^{124}Sb, ^{110m}Ag, and ^{65}Zn.

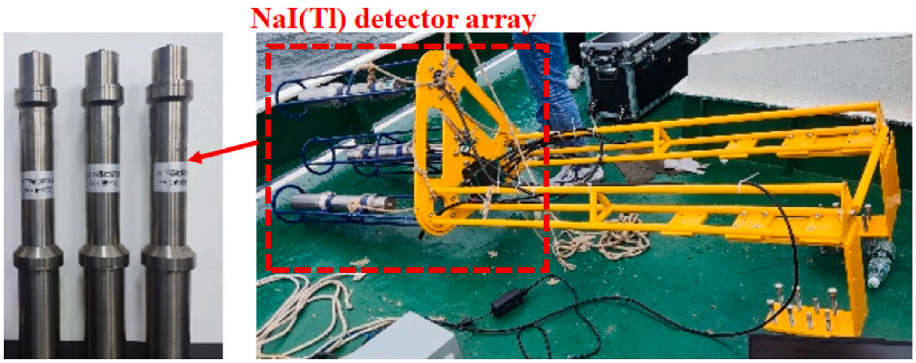

Fig. 9. NaI(Tl) detector array and bracket.

were able to withstand water pressure at a depth of 200 m, so they could be mounted on a longer bracket to detect seawater radioactivity at greater depths in the future. The outer shell of the NaI(Tl) detectors was made of Ti alloy, which has the characteristics of corrosion resistance and impact resistance. Additionally, the mounting bracket could also protect the detectors. Because of the above reasons, these NaI(Tl) detectors could withstand abuse from a moving ship in a storm or colliding with an object.

The online monitoring system for navigable marine radioactivity primarily consisted of an underwater radiation detector array, air dose rate meter, meteorological sensors, data acquisition devices, communication systems, and positioning systems, as illustrated in Fig. 10. The acquisition and communication module was one of the core components of the entire system, and their hardware and software were self-made. The collection module automatically collects and packages data from detector arrays, air dose rate meter, and meteorological sensors at regular intervals, including environmental monitoring data such as seawater dose rate, seawater gamma spectrum, air dose rate, temperature, wind speed, air pressure and location. The collection frequency can be adjusted online, with a range from every 30 s to every 24 h. The communication module transmits these data to the remote server through a 4/5G wireless network. If there is no wireless network, data can also be directly transmitted to a portable laptop through a wired connection. Finally, the software on the server would process these data, utilizing spectral analysis methods such as nuclide identification and activity concentration calculation. The software interface can display real-time information, including seawater γ dose rates, seawater γ spectra, and location.

3.2. Experimental verification of the volume-efficiency curve

The volume-efficiency curve of the NaI(Tl) detector array, as fitted in Section 2.3, was verified in the standard liquid sources provided by the National Ocean Technology Center, China. The standard liquid source was placed in a water tank with a height of 3 m and a diameter of 2.5 m, which contained ^{137}Cs (0.85 Bq/L) and ^{133}Ba (0.36 Bq/L). Each detector in the array was placed at the center of the water tank, with the NaI(Tl) crystal positioned 1 m below the water surface, and measured for 1 h in the standard liquid source. The counts at the same channel address in the energy spectra from three detectors were summed to obtain the synthetic spectra, as shown in Fig. 11.

The volume-efficiencies ε_V for ^{137}Cs and ^{133}Ba at 662 and 356 keV, respectively, were obtained from the volume-efficiency curve shown in Fig. 8, which yielded 1.22 cps/(Bq/L)@662 keV and 1.34 cps/(Bq/L) @356 keV. The formula for calculating the nuclide activity concentration is shown as Formula (3).

$$a = \frac{n}{\varepsilon_V p} \tag{3}$$

where a is the activity concentration in Bq/L, n is the net count rate of the full energy peak in cps, and p is the gamma-ray emission probability. As shown in Table 3, the bias of the activity concentrations for ^{137}Cs and ^{133}Ba were less than 5%, which indicates that the efficiency calibration is reasonably accurate.

3.3. Minimum detectable activity concentration calculation of the underwater radiation detector array

Minimum detectable activity concentration (MDC) is a substantial performance indicator of the detection instrument, which refers to the

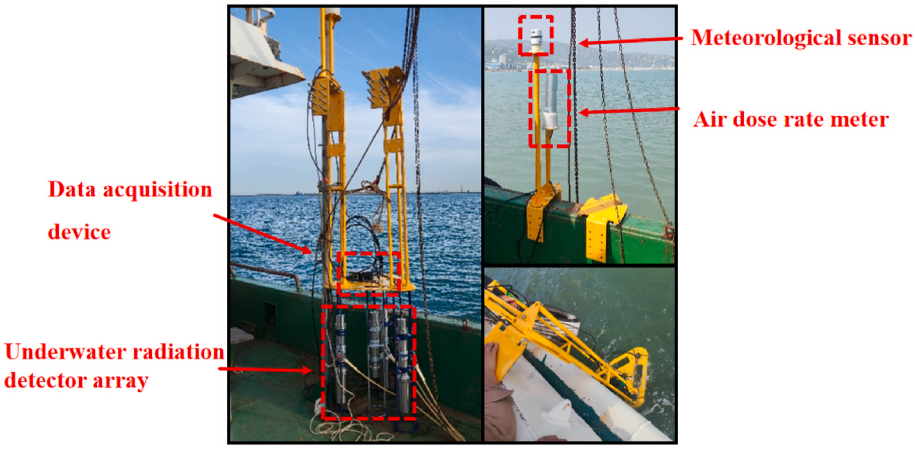

Fig. 10. Navigable online monitoring system.

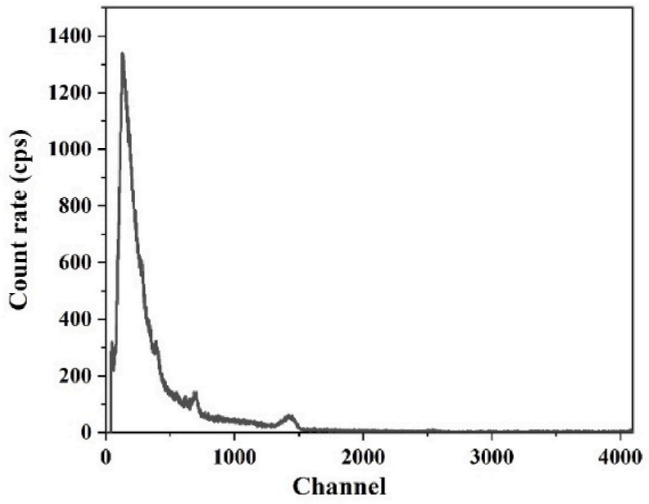

Fig. 11. Composite gamma-ray spectrum measured for 1 h.

Table 3
Computed results for the activity concentrations of ^{137}Cs and ^{40}K.

Nuclide	Actual activity concentrations (Bq/L)	Measured activity concentrations (Bq/L)	Bias
^{137}Cs	0.85	0.829	2.47%
^{133}Ba	0.36	0.358	0.50%

minimum activity concentration that the system can detect. The accepted calculation formula of MDC is shown as Formula (4) [18,19]:

$$MDC = \frac{2.65 + 4.71\sqrt{B}}{\varepsilon_V p T} \tag{4}$$

where B represents background counts, and the ROIs for background counts B were determined as the regions covering an energy interval of 2.5 × FWHM, centered on the photon energy for the radionuclides; p stands for gamma emission probability; T is the duration of spectral measurement; and ε_V denotes volume-efficiency, which was calculated by the fitting curve in Section 2.3. Based on the gamma spectrum measured by the NaI(Tl) detector array in seawater, the MDC for the radionuclides was calculated, as shown in Table 4. In this study, only the presence of a single radioactive nuclide was considered, therefore the results of MDCs in Table 4 are theoretically the lowest.

The volume-efficiencies and MDCs of the individual detector and detector array for ^{137}Cs were compared, as shown in Table 5. The volume-efficiency of the individual detector was calculated based on formula (1). The energy spectrum of each detector had been processed through energy calibration. Hence, the background counts RoIs of the detector array could be obtained by summing the ROIs of the three detectors. The results indicated that the sum of the volume-efficiencies of the three detectors was 1.23 cps/(Bq/L), slightly higher than the 1.22 cps/(Bq/L) from the detector array, with a deviation of 0.82%. For MDCs, although the background counts of the detector array had increased, due to the square root processing of the background counts during calculation, the MDCs of the detector array were smaller than that of a single detector. The detector array can detect lower activity concentrations of radioactive nuclides at the same measurement time. The optimization of the detector array scheme can maximize the effectiveness of each detector in the array, thereby enhancing the volume-efficiency and detectability for artificial radionuclides.

Table 4
MDC of radionuclides under different spectral acquisition times.

Nuclide	300 s (Bq/L)	600 s (Bq/L)	1800 s (Bq/L)	1 h (Bq/L)	24 h (Bq/L)
^{131}I	0.2304	0.1629	0.0941	0.0665	0.0136
^{60}Co	0.0725	0.0512	0.0296	0.0209	0.0043
^{137}Cs	0.1522	0.1076	0.0621	0.0439	0.0090
^{134}Cs	0.1501	0.1061	0.0613	0.0433	0.0088
^{124}Sb	0.2092	0.1480	0.0854	0.0604	0.0123
^{208}Tl	0.1047	0.0740	0.0427	0.0302	0.0062
^{40}K	0.8757	0.6192	0.3575	0.2528	0.0516
^{214}Bi	0.6614	0.4677	0.2700	0.1909	0.0390

3.4. Experimental results of seawater radioactivity measurement

The system was used to conduct two application tests in the sea near the Tianwan nuclear power plant in Lianyungang, including nearshore and offshore areas. Each test involved 3 h of sailing at a speed of 5 km/h, with seawater gamma spectroscopy collected every 5 min. In addition, the background spectrum measured for 30 min was obtained by an in situ measurement experiment near the nuclear power plant, with the position retained during the measurement. Fig. 12 shows the background gamma spectra measured for 5 min.

During the deployment tests, the identification rate for ^{40}K isotopes was 100%, with an average activity concentration of 11.4 Bq/L. Other natural isotopes were not identifiable due to their lower concentrations and shorter measurement times. No artificial isotopes, such as ^{137}Cs, were detected during the tests. The MDC values for ^{137}Cs for 5 and 30 min measurement were 0.152 and 0.062 Bq/L. The average activity of ^{137}Cs in the seawater near the Tianwan nuclear power plant has been reported to be around 0.012 Bq/L, which was lower than the MDC of the proposed system [20]. However, the proposed system can effectively detect marine radioactive pollution accidents with relatively high radioactivity in a timely way.

The seawater samples obtained near the Tianwan nuclear power plant were also analyzed in the laboratory using a high-purity germanium gamma spectrometer [21,22]. Table 6 shows the radioactivity concentrations of ^{40}K from both methods. The measurement results showed that the relative errors ranged from 3.6% to 21.3%, which verified the feasibility and reliability of the system.

4. Conclusion

This study proposed a navigable online monitoring system equipped with multiple large-volume NaI(Tl) detectors. This system could monitor a wide range of seawater radioactivity in a short period. While keeping the total volume of the NaI(Tl) crystals constant, Monte Carlo simulations were employed to optimize the number of NaI(Tl) crystals and the detector spacing in the underwater radiation detector array to enhance the volume-efficiency of the system. Simulation results indicated that, for the NaI(Tl) crystal with a total volume of 127.2 cubic inches, dividing it into three or four crystals and arranging them in a detector array with a detector spacing of over 30 cm were more suitable for the monitoring of seawater radioactivity.

Based on the simulation results, three Φ3" × 6″ NaI(Tl) detectors and the bracket with a fixed detector spacing of 30 cm were fabricated. The volume-efficiency for ^{137}Cs of the system reached 1.22 cps/(Bq/L) and was about six times higher than from a buoy-based monitoring system with a Φ3" × 3″ NaI(Tl) detector. The simulated volume-efficiency curve was verified using standard liquid sources. The results showed that the relative error between the measured values and the actual activity concentration was within 5%, which verified the accuracy of the volume-efficiency derived from the simulated efficiency curve. The deployment tests were performed in the sea area near the Tianwan nuclear power plant in Lianyungang, which confirmed the accuracy and stability of the system. The test results showed that the average activity concentration of ^{40}K was 11.4 Bq/L, which was consistent with the laboratory analysis results. Therefore, the stability and reliability of the system were verified. The MDC of the system for ^{137}Cs for 5 min

Table 5
Volume-efficiencies and MDCs of the individual detector and the detector array for ^{137}Cs.

Detector	volume-efficiency for ^{137}Cs (cps/(Bq/L))	ROIs for background counts *B* for 300s (cps)	MDCs for 300s (Bq/L)	ROIs for background counts *B* for 1800s (cps)	MDCs for 1800s (Bq/L)
#1 detector	0.4100	40	0.3072	199	0.1089
#2 detector	0.4100	34	0.2853	208	0.1123
#3 detector	0.4100	19	0.2198	185	0.1051
detector array	1.2200	93	0.1522	592	0.0621

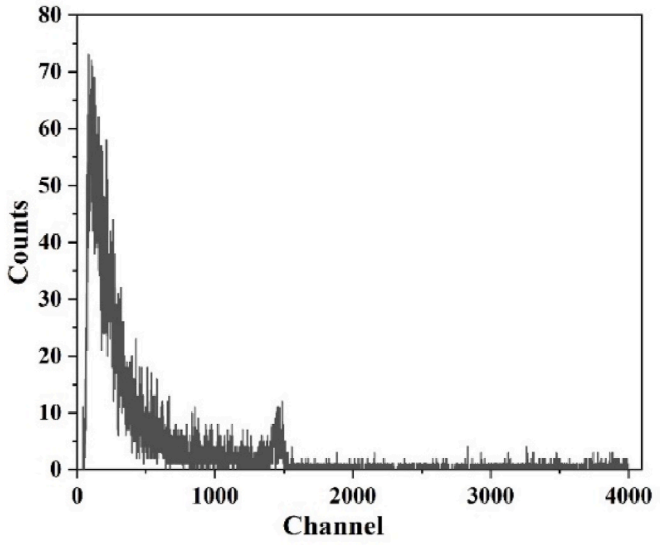

Fig. 12. Background spectrum measured for 5 min.

Table 6
Activity concentration of ^{40}K.

Sample name	Navigable monitoring (Bq/L)	Laboratory measurement (Bq/L)	Bias
Nearshore location 1	11.3	13.2	14.4%
Nearshore location 2	11.7	9.4	21.3%
Offshore location 1	10.6	11.0	3.6%
Offshore location 2	12.1	10.6	14.2%

measurement reached 0.152 Bq/L.

In addition to the issues discussed in this paper, the poor resolution of NaI(Tl) detector will make the system difficult in identify multiple radionuclides. In the future, a high-resolution HPGe detector can be installed on the same ship for a quick isotope identification from grab sample.

CRediT authorship contribution statement

Yihang Shou: Writing – review & editing, Writing – original draft, Visualization, Investigation, Formal analysis. **Pin Gong:** Writing – review & editing, Validation, Project administration, Funding acquisition, Formal analysis, Data curation, Conceptualization. **Jinzhao Zhang:** Writing – review & editing, Visualization, Methodology, Data curation. **Zeyu Wang:** Writing – review & editing, Methodology, Data curation. **Dajian Liang:** Visualization, Methodology, Funding acquisition, Data curation. **Cheng Zhou:** Supervision, Project administration, Funding acquisition. **Xiaobin Tang:** Writing – review & editing, Supervision, Funding acquisition.

Declaration of competing interest

The authors declare that they have no known competing financial interests or personal relationships that could have appeared to influence the work reported in this paper.

Data availability

Data will be made available on request.

Acknowledgments

This work was supported by the Primary Research and Development Plan of Jiangsu Province (Grant No. BE2023816, BE2022846), and the Research project of General Administration of Customs (Grant No. 2024HK088).

References

[1] F. Kaviani, M.H. Memarian, M. Eslami-Kalantari, Radioactive impact on Iran and the world from a postulated accident at bushehr nuclear power plant, Prog. Nucl. Energy 142 (2021) 103991, https://doi.org/10.1016/j.pnucene.2021.103991.
[2] J. Vives i Batlle, The potential impact of marine discharges from Fukushima 10 years after the accident, Integrated Environ. Assess. Manag. 18 (2022) 1530–1538, https://doi.org/10.1002/ieam.4592.
[3] A.A. Sarkisov, V.L. Vysotskii, The largest nuclear accident in the history of the nuclear fleet. Reconstruction of events and analysis of the accident consequences to assess the risks and hazards of small nuclear power facilities, Nucl. Eng. Des. 384 (2021) 111440, https://doi.org/10.1016/j.nucengdes.2021.111440.
[4] B. Nogrady, Is Fukushima wastewater release safe? What the science says, Nature (2023), https://doi.org/10.1038/d41586-023-02057-y.
[5] M. Yii, A. Zaharudin, M. Norfaizal, Concentration of radiocaesium 137Cs and 134Cs in sediments of the Malaysian marine environment, Appl. Radiat. Isot. 65 (2007) 1389–1395, https://doi.org/10.1016/j.apradiso.2007.07.002.
[6] H. Baltas, E. Kiris, M. Sirin, Determination of radioactivity levels and heavy metal concentrations in seawater, sediment and anchovy (Engraulis encrasicolus) from the Black Sea in Rize, Turkey, Mar. Pollut. Bull. 116 (2017) 528–533, https://doi.org/10.1016/j.marpolbul.2017.01.016.
[7] S. Uddin, M. Behbehani, A. Aba, Radioactivity in seawater–A review from Kuwait, Athens Journal of Sciences 2 (2015) 265–273, https://doi.org/10.30958/ajs.2-4-3.
[8] P. Povinec, J. La Rosa, S. Lee, S. Mulsow, I. Osvath, E. Wyse, Recent developments in radiometric and mass spectrometry methods for marine radioactivity measurements, J. Radioanal. Nucl. Chem. 248 (2001) 713–718, https://doi.org/10.1023/A:1010696813200.
[9] C. Tsabaris, E.G. Androulakaki, S. Alexakis, An optimized quantification method for marine radioactivity measurements: application in the southern caspian sea using the KATERINA underwater γ-spectrometer, J. Mar. Sci. Eng. 11 (2023) 725, https://doi.org/10.3390/jmse11040725.
[10] J.H. Lee, J.I. Byun, D.M. Lee, A two-point in situ method for simultaneous analysis of radioactivity in seawater and sediment, J. Radioanal. Nucl. Chem. 322 (2019) 639–648, https://doi.org/10.1007/s10967-019-06774-5.
[11] C. Wedekind, G. Schilling, M. Grüttmüller, K. Becker, Gamma-radiation monitoring network at sea, Appl. Radiat. Isot. 50 (1999) 733–741, https://doi.org/10.1016/S0969-8043(98)00062-1.
[12] S.Y. Han, S. Maeng, H.Y. Lee, S.H. Lee, Preliminary study on the detection efficiency and estimation of minimum detectable activity for a NaI(Tl)-based seawater monitoring system, J. Environ. Radioact. 218 (2020) 106222, https://doi.org/10.1016/j.jenvrad.2020.106222.
[13] J. Song, P. Gong, P. Wang, J. Zhang, Z. Hu, C. Zhou, X. Zhu, Q. Wei, J. Zhou, X. Tang, Unmanned stationary online monitoring system based on buoy for marine gamma radioactivity, Appl. Radiat. Isot. 191 (2023) 110528, https://doi.org/10.1016/j.apradiso.2022.110528.
[14] J. Hao, Y. Zhang, B. Wu, X. Feng, Research and development of key technologies for in-situ monitoring of marine radioactive gamma spectroscopy, in: Third International Conference on Digital Signal and Computer Communications (DSCC 2023), 2023, pp. 430–436, https://doi.org/10.1117/12.2685550. SPIE.

[15] J.I. Byun, S.W. Choi, M.H. Song, B.U. Chang, Y.J. Kim, J.Y. Yun, A large buoy-based radioactivity monitoring system for gamma-ray emitters in surface seawater, Appl. Radiat. Isot. 162 (2020) 109172, https://doi.org/10.1016/j.apradiso.2020.109172.

[16] R. Casanovas, J. Morant, M. Salvadó, Development and calibration of a real-time airborne radioactivity monitor using direct gamma-ray spectrometry with two scintillation detectors, Appl. Radiat. Isot. 89 (2014) 102–108, https://doi.org/10.1016/j.apradiso.2014.01.026.

[17] Z. Yanxia, L. Jin, L. Jiacheng, H. Shanbiao, Y. Zhengwei, Discussion on monitoring items of radionuclides in influents from nuclear power plants, Radiat. Protect. 34 (2014) 390–394. https://inis.iaea.org/search/search.aspx?orig_q=RN:49042776.

[18] J. Kirkpatrick, W. Russ, R. Venkataraman, B. Young, Calculation of the detection limit in radiation measurements with systematic uncertainties, Nucl. Instrum. Methods Phys. Res., Sect. A 784 (2015) 306–310, https://doi.org/10.1016/j.nima.2015.01.005.

[19] C. Bagatelas, C. Tsabaris, M. Kokkoris, C. Papadopoulos, R. Vlastou, Determination of marine gamma activity and study of the minimum detectable activity (MDA) in 4pi geometry based on Monte Carlo simulation, Environ. Monit. Assess. 165 (2010) 159–168, https://doi.org/10.1007/s10661-009-0935-4.

[20] H. Liu, K. Jiang, Z. Wang, K. Sun, Analysis and evaluation of 137 Cs activity concentrations in the seawater near Tianwan nuclear power station, Radiat. Protect. 37 (2017) 369–373. qikan.cqvip.com/Qikan/Article/Detail?id=673316163.

[21] S.F. Ozmen, O. Güven, Sediment radioactivity levels of deep-water fishery grounds in antalya bay, Aquatic Sciences and Engineering 36 (2021) 29–33, https://doi.org/10.26650/ASE2020714512.

[22] T. Mimura, M. Mimura, C. Komiyama, M. Miyamoto, A. Kitamura, Measurements of gamma (γ)-emitting radionuclides with a high-purity germanium detector: the methods and reliability of our environmental assessments on the Fukushima 1 Nuclear Power Plant accident, J. Plant Res. 127 (2014) 91–97, https://doi.org/10.1007/s10265-013-0594-y.